Correlation modeling between process condition of sandblasting and surface texture: A multi-scale approach

Hsin Shen Ho, Maxence Bigerelle, Renald Vincent, Raphaël Deltombe

SCANNING VOL. 38, 191–201 (2016)

Correlation Modeling Between Process Condition of Sandblasting and Surface Texture: A Multi-Scale Approach

Hsin Shen Ho,[1,2] Maxence Bigerelle,[3] Renald Vincent,[2] and Raphael Deltomb[3]

[1]School of Mechanical Engineering, Zhengzhou University, 100 Science Road, Zhengzhou, China
[2]Pole EME, Centre Technique des Industries Mécaniques, 52 avenue Félix Louât, Senlis, France
[3]Equipe Matériaux, Surfaces et Mise en forme, TEMPO, LAMIH, Université de Valenciennes, Campus Mont Houy, Valenciennes Cedex 9, France

Summary: In the present study, the influence of sandblasting condition (working pressure) on surface texture is modeled, relying on a multi-scale approach and statistical analysis. To improve the correlation modeling between the process condition and surface texture, special effort is made to identification of an optimal parameter set, including 3D roughness parameters, cut-off lengths, filter types and model types. A power law relationship is identified between the pressure and S_{dq} computed with a cut-off length of 120 μm using a low-pass filter. Experimental and theoretical arguments are provided for justification. SCANNING 38:191–201, 2016. © 2015 Wiley Periodicals, Inc.

Key words: surface finishing, surface topography, multi-scale analysis, statistical analysis

Introduction

Sandblasting is one of the commonly used surface treatment methods. It is traditionally used for surface cleaning and rust removal, nowadays is widely applied to increase the surface roughness on the micro-scale level to facilitate cell adhesion (Anselme and Bigerelle, 2005), and improve surface bonding (Rodrigues *et al.*, 2009) and surface wettability (Kim *et al.*,2012).

Surface characterization has received much attention for the purpose of modelling the cause-effect relation between the surface texture and its functional application. Considering the complexity and irregularity of the surface texture (e.g., by sandblasting), one of the major difficulties in such work consists in identifying an appropriate scale that can reveal the features of the micro-complexity of the surface texture. The multi-scale analysis, defined using the fractal theory (Mandelbrot, '77), is therefore implemented in numerous work, such as Brown and Siegmann (2001), Vulliez *et al.* (2014) and Berglund *et al.* (2010a, 2010b). They reported correlations between surface roughness and functional properties, and these correlations vary with respect to scale.

As to the roughness parameters for surface characterization, the arithmetic mean deviation (R_a) is commonly used as the only candidate for surface texture analysis in academic and industrial fields. For instance, R_a is exhibited to be a promising parameter to describe the textures of polished surfaces in optical appliance applications (Shiou and Asmare, 2015) and of machined surfaces in aerospace applications (Xu *et al.*, 2015). However, this roughness parameter may appear insufficient to tackle the complexity of other engineering surface textures, hence additional roughness parameters of ISO are needed (Nowicki, '85; Bigerelle *et al.*, 2013), even new roughness parameters are developed by users for their specific applications (Anselme and Bigerelle 2005; Vulliez *et al.*, 2014). In spite of the proliferation of new roughness parameters, very often, not all of them are fully utilized for texture analysis, which is termed by Whitehouse ('94) as "parameter rash". This ignorance seems to be a consequence of the fact that not many studies incline to question the pertinence of the roughness parameters which are used to describe surface textures, therefore effort is made to address such issue in the present work. Moreover the three dimensional (3D) roughness parameters are considered and analyzed, which are believed to provide richer information compared to ones of 2D (Nwaogu *et al.*, 2013).

Surface characterization for the correlation modeling between the process condition and the resulted

Address for reprints: H. S. Ho, School of Mechanical Engineering, Zhengzhou University, 100 Science Road, 450001 Zhengzhou, China
E-mail: hsinshen.ho@zzu.edu.cn

Received 24 April 2015; Accepted with revision 21 July 2015

DOI: 10.1002/sca.21254
Published online 6 August 2015 in Wiley Online Library (wileyonlinelibrary.com).

surface texture is the main concern of the present work, with the ultimate aim to obtain the desirable surface texture by controlling the process condition. The sandblasting process parameters such as duration, angle and size of abrasives are frequently used to alter the texture of sandblasted surfaces. Qualitative assessments have been performed to describe the effect of those process conditions on surface texture (Bouzid and Bouaouadja, 2000; Zhou *et al.*, 2011; Wang *et al.*, 2014). For instance, the maximum height of the profile (R_t) is exhibited to increase linearly with impact angle and blasting duration (Bouzid and Bouaouadja, 2000), and R_a is reported to increase with blasting duration (Zhou *et al.*, 2011) and size of abrasives (Wang *et al.*, 2014).

The contributions of the present study are as follows: first, a multi-scale analysis is carried out in order to reveal the inherent feature of the sandblasted texture, considering two (low and high) Gaussian filters together with a series of cut-off lengths; second, the bootstrap method is implemented to quantify the aleatory uncertainty of surface data, assuming them to be isotropic; third, attempt is made to obtain a quantitative correlation between the sandblasting condition and resulted surface texture based on regression analysis; fourth, considering all the 3D roughness parameters of ISO25178-2 and EUR 15178N, a computational protocol is established to identify a most relevant parameter set, including 3D roughness parameters, scale, filter type and regression model, for modeling the effect of the sandblasting condition on the surface texture. The proposed methodology is finally applied to the sandblasted surface of stainless steel AISI 304L with the working pressure as the process parameter.

The remainder of the paper is organized as follows. Section Material and Measurement Method presents the material and method used in this work. Section Computational Protocol describes the computational protocol dedicated to identifying the optimal parameter set for textures analysis, including 3D roughness parameter, evaluation scale, filter type and regression model. Section Results and Discussion is devoted to analyzing the surface textures, the relevance of the obtained optimal parameters set is discussed. Concluding remarks are given in Section Conclusions.

Material and Measurement Method

Material and Sandblasting Process

In this study, the stainless steel AISI 304L is the target material, which has the following chemical composition (% in weight): C (0.022), Mn (1.58), Si (0.35), S (0.024), P (0.039), Ni (8.08), Cr (18.60), Mo (0.39), Cu (0.60), N (0.046) and Fe (base). Seven substrates are prepared; each of them is a 5 mm thick cylindrical plate with a diameter of 50 mm. These substrates are automatically polished with pre-defined experimental settings (load: 150 N, duration: 3 min), a mirror surface is obtained using a diamond paste of 3 μm.

Substrates are blasted in a sandblasting machine CSF 70 V by silicon carbide (SiC) particles with diameters ranging from 0.15 mm to 0.25 mm. Fixing the angle (90°), the distance (5 cm) and the duration (60 s) of the sandblasting process, the effect of the working pressure is in particular investigated on the surface texture by setting its value as: 1, 2, 3, 4, 5, 6, and 7 bar(s).

Roughness Measurement and Estimation

Roughness measurements are conducted with a three-dimensional non-contact optical profilometer (Zygo NewView™ 7300, Zygo Corp.). The white light interferometer (20× Mirau objective) is equipped with a high speed camera (320 × 240 pixels). The optical resolution is 710 nm in x, y directions, which is related to the numerical aperture of the objective and achieved through the Sparrow criterion. The sampling interval is 1.09 μm. Setting the working distance as 4.70 mm, a region of 0.35 mm × 0.26 mm is measured. A total of 16 individual measurements are stitched together with an overlap of 20%, producing a stitched region of 1.19 mm × 0.89 mm for reliable roughness measurement. Twenty stitched regions are created per substrate.

In order not to affect the micro-geometry of surfaces, the geometrical form is removed by rectifying the measured surfaces with a third degree polynomial fitting; the reduction of the residual variance is insignificant when increasing the polynomial degree from two to four (Mezghani *et al.*, 2009). To fully characterize the measured surface texture, a total of 55 3D roughness parameters are computed in agreement to ISO 25178-2 (2012) and EUR 15178N (1993). In addition, the edge effect of measured surfaces is properly managed for the reliability and accuracy of the roughness estimates. The roughness parameters are listed in Table I, which are discussed later for their relevance for the characterization of the sandblasted surfaces.

Computational Protocol

The present study is conducted based on a proposed computational protocol that relies on a multi-scale technique integrated with computer-based bootstrap method (see Fig. 1). It is elaborated in the following sections.

TABLE I Surface roughness parameters used in the present study

ISO 25178 (2012)		
Amplitude parameters		
S_a	Arithmetic mean height	$S_a = \frac{1}{A}\iint_A \lvert z(x,y)\rvert dxdy$ with A being the definition area
S_q	Root mean square height of the surface	$S_q = \sqrt{\frac{1}{A}\iint z^2(x,y)\mathrm{d}x\mathrm{d}y}$ with A being the definition area
Spatial parameters		
S_{al}	Auto-correlation length	$S_{al} = \min_{tx,ty\in R}\sqrt{tx^2+ty^2}$ where $R = \{(tx,ty) : ACF(tx,ty) \le s, 0 \le s < 1\}$
S_{tr}	Texture-aspect ratio	$S_{tr} = \frac{\min_{tx,ty\in R}\sqrt{tx^2+ty^2}}{\max_{tx,ty\in Q}\sqrt{tx^2+ty^2}}$ where $R = \{(tx,ty) : ACF(tx,ty) \le s, 0 \le s < 1\}$ $Q = \{(tx,ty) : ACF(tx,ty) \ge s{**}\}$
**denotes the property that the $ACF \ge s$ on the straight line connecting the point (tx,ty) to the origin		
Hybrid parameters		
S_{dq}	Root mean square gradient	$S_{dq} = \sqrt{\frac{1}{A}\iint_A \left[\left(\frac{\partial z(x,y)}{\partial x}\right)^2 + \left(\frac{\partial z(x,y)}{\partial y}\right)^2\right] dxdy}$ with A being the definition area
S_{dr}	Developed interfacial area ratio	$S_{dr} = \frac{1}{A}\left[\iint_A \left(\sqrt{\left[1+\left(\frac{\partial z(x,y)}{\partial x}\right)^2 + \left(\frac{\partial z(x,y)}{\partial y}\right)^2\right]} - 1\right) dxdy\right]$ with A being the definition area
EUR 15178N (1993)		
Functional indices		
S_{bi}	Surface bearing index	$S_{bi} = \frac{S_q}{\mathrm{Trueheight}(0.05)}$

Multi-Scale Technique

The multi-scale technique is performed with the use of two types (high-pass and low-pass) of Gaussian filters together with 23 cut-off lengths ranging from 5 μm to 1000 μm to separate surface roughness from surface waviness at different wavelengths. Figure 6 (A–B) illustrate the effects of coupling of filter type and cut-off length on measured surfaces shown in Figure 2, it is observed that filter type and cut-off length can affect significantly surface texture.

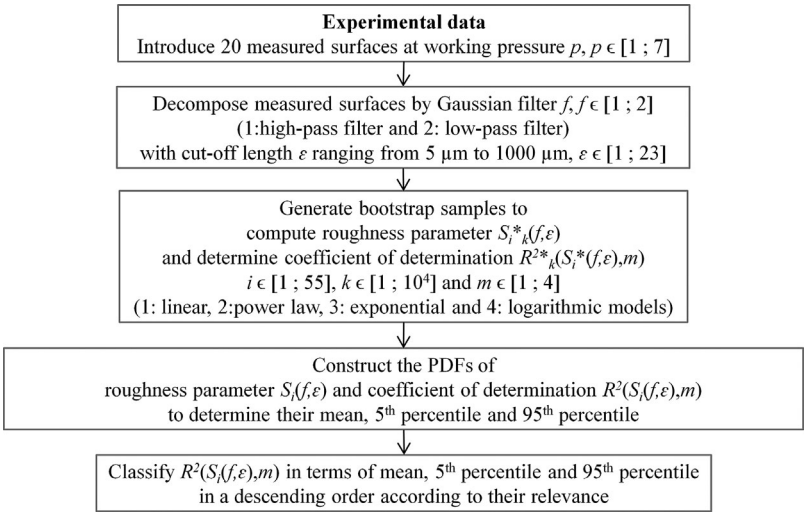

Fig 1. Framework of the methodology proposed for identifying the optimal parameter set. $S_i^*{}_k(f,\varepsilon)$ denotes the roughness parameter S_i estimated based on kth surface sample with the filter type (f) and cut-off length (ε).

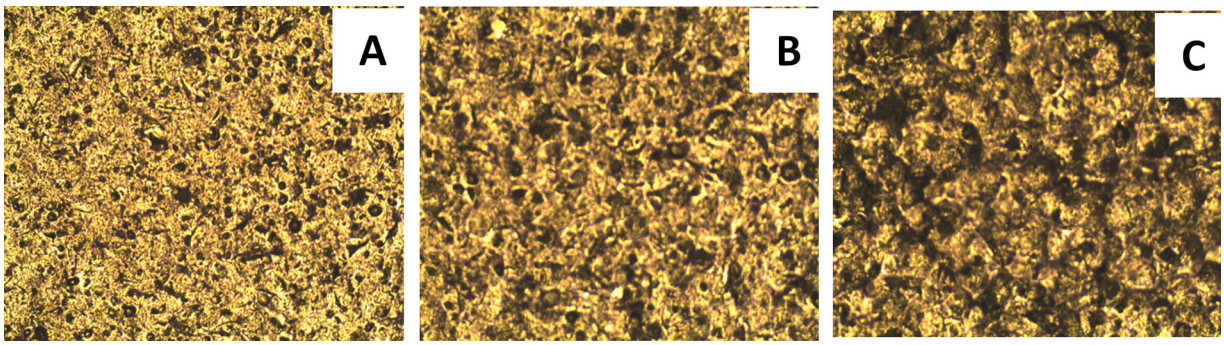

Fig 2. Optical micrographs of surfaces blasted at 1 (A), 3 (B), 7 (C) bars.

Computer-Based Bootstrap Method

Due to the limited amount of available experimental data, the computer-based bootstrap method is adopted, which, relying on the resampling technique, consists in generating a high number of simulated bootstrap samples by randomly sampling with data replacement from the original experimental data set (Efron, '79).

Applying the bootstrap method to the 20 stitched surface regions, 10^4 bootstrap samples are generated, based on which all the roughness parameters are computed with different settings of filter type and cut-off length. Subsequently, the correlation between each computed roughness parameter and the working pressure is assessed based on four types of regression models, which are linear, power, exponential and logarithm models. The coefficient of determination R^2, with a value$\in$[0;1], is invoked here to indicate the model quality as it is demonstrated to be highly capable of providing the goodness-of-fit summary statistic for a large variety of mathematical regression models (Cameron and Windmeijer, '97). It has been employed to find the best scale for characterizing relative area with adhesion (Brown and Siegmann, 2001) and for correlating curvature with fatigue limit (Vulliez *et al.*, 2014).

Optimal Parameter Set

For every scale, filter type and regression model, the probability density functions (PDFs) of each roughness parameter and its related coefficient of determination are empirically constructed from the simulated bootstrap surface samples. Their descriptive statistics such as mean, 5th percentile and 95th percentile are also derived. Collect all the coefficients of determination computed with different parameter combinations and class them in terms of mean, 5th percentile and 95th percentile in a descending order, the pertinence of the parameter set is simply demonstrated by the classification order, which refers to the goodness-of-fit of the parameter set for the underlying law governing the sandblasting process. The acceptance of the most relevant parameter set is based on the highest mean value of the coefficient of determination.

Results and Discussion

Results

Measured surface analysis

Figure 2 and Figure 3 illustrate surfaces of stainless steel AISI 304L substrates after sandblasting. It is shown that sandblasting results in the formation of ragged surfaces, i.e. the surface texture (c.f. Fig. 2) and roughness level (c.f. Fig. 3) of blasted substrates are greatly modified, implying that they are significantly dependent on impact pressure.

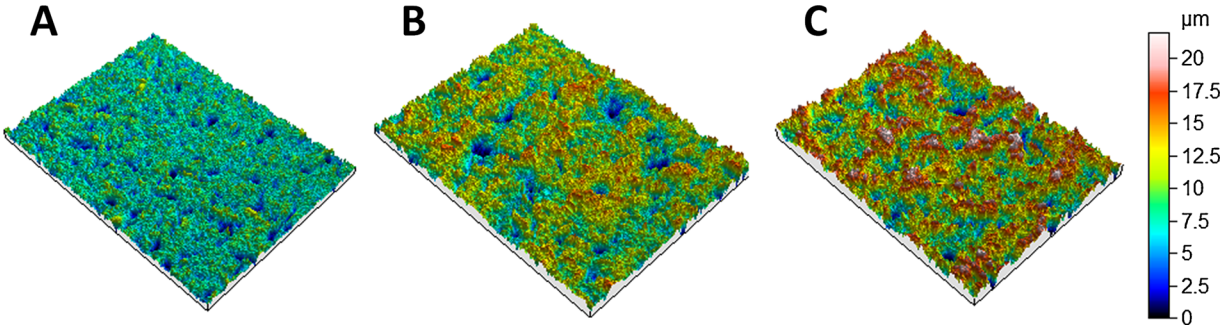

Fig 3. 3D representation of surfaces blasted at 1 (A), 3 (B), 7 (C) bars.

Optimal parameter set

Based on the multi-scale technique integrated with computer-based bootstrap method, the relevance of more than 10^4 possible combinations, consisting of 55 roughness parameters, two filter types, 23 cut-off lengths and four regression models, is assessed to seek an optimal parameter set for the description of the functional correlation between the working pressure and surface roughness.

Figure 4(A–D) illustrates all the possible combinations of parameters that are sorted in a descending order according to their relevance indicated by the coefficient of determination (R^2). The mean of R^2 is up to 0.99, suggesting the presence of an optimal parameter set: the power law function describes best the interrelationship between the working pressure and the roughness parameter called root mean square surface slope (S_{dq}) computed at the cut-off length of 120 μm using a low-pass filter (refer to Fig. 5). This finding is found to be in accordance with Berglund *et al.* (2010a) where S_{dq} varies with scale.

The evolution of S_{dq} is given as a function of the pressure in Figure 5; S_{dq} exhibits a tendency of monotonically increasing with the pressure. Indeed, when the pressure increases, the particle impact on the substrate's surface becomes stronger, leading to the formation of wider craters and deeper indents, and consequently the local slope of each facet and its orientation become larger. The fact that the fitted curve goes through the confidence intervals implies that the found optimal parameter set is suitable for the description of the correlation between the surface roughness and working pressure.

Result illustration

Filter type. The surface textures obtained with the use of a high-pass filter and low-pass filter together with three cut-off lengths (μm: 22, 120, 1000 - full horizontal scale) for three working pressures (bar(s): 1, 3, 7) are represented in Figure 6(A and B), respectively. The impact of abrasive particles on the substrate surfaces is observed to be isotropic regardless of filter types, implying that sandblasted surfaces have the same characteristics in all directions. Figure 6(A), representing surfaces obtained with a high-pass filter and 120 μm, shows that the size of impact craters increases with increasing working pressure. Figure 6(B), illustrating surfaces obtained with a low-pass filter, reveals the presence of macro-waviness at full horizontal scale and reflects the geometry of the abrasive particles used for sandblasting at 120 μm; the use of a low-pass filter neglects the phenomenon of localized deformation of a surface.

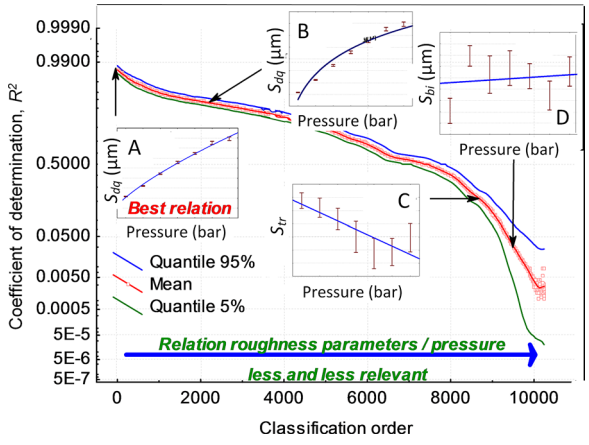

Fig 4. Classification order of the relevance of parameter sets for modeling the pressure effect on the surface texture. Modeling of S_{dq} with the power law function (A) and logarithmic function (B) at a cut-off length of 120 μm and modeling of S_{tr} (C) and S_{bi} (D) with the linear function at a full horizontal scale, using a low-pass filter.

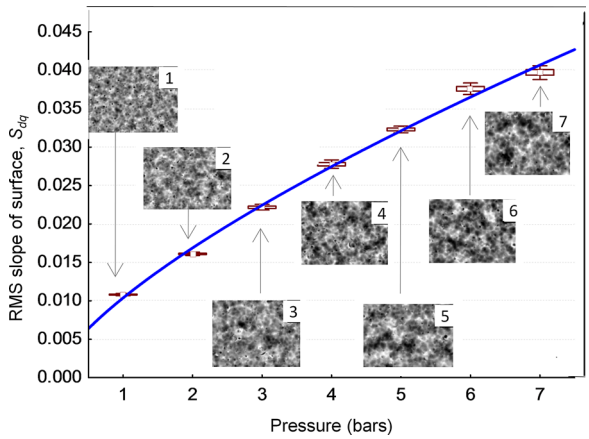

Fig 5. Modeling of S_{dq} and working pressure with power law function for a cut-off length of 120 μm using a low-pass filter.

Scale. In Figure 7, the value of R^2 for the modeling of S_{dq} with the power law model using a low-pass filter is computed as a function of the scale varying from 10 μm to 1000 μm; R^2 is exhibited to be a convex function of the scale. 120 μm is exhibited to be the optimal scale. And other scales, such as 10 μm and 1000 μm, describe the characteristics of sandblasted surfaces in a suboptimal sense.

Roughness parameter. Figure 8 shows the PDFs of S_{dq} for the examined seven working pressures, computed at the relevant scale using pertinent filter type. The PDFs are perfectly disconnected for the seven pressures, implying that S_{dq} is capable of describing the pressure effect on the surface texture.

Regression model. Figure 9(A-D) illustrate the modeling of S_{dq} and the working pressure based on linear, logarithmic, exponential and power law functions. As indicated by R^2, the power law model in Figure 9(D) exhibits the best performance (with $R^2 = 0.995$) in comparison to the linear model (with $R^2 = 0.970$ in Fig. 9(A)), logarithmic model (with $R^2 = 0.935$ in Fig. 9(B)) and exponential model (with $R^2 = 0.925$ in Fig. 9(C)).

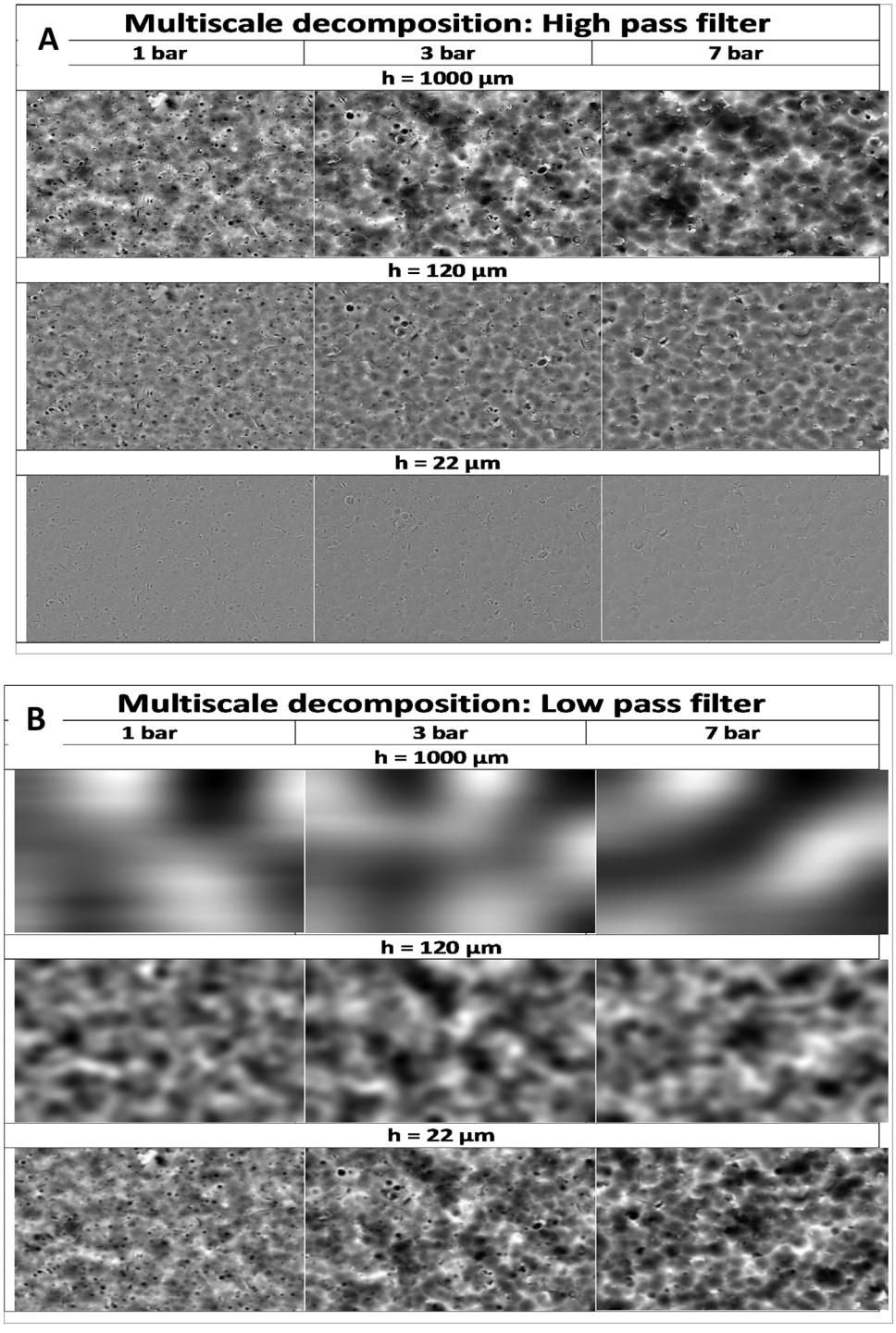

Fig 6. Textures of surfaces blasted at the working pressures (bar(s): 1, 3, 7) with the use of a high-pass filter (A) and a low-pass filter (B) together with cut-off lengths equal to 22 µm, 120 µm and 1000 µm.

To further illustrate the relevance of obtained results, another two roughness parameters calculated over the full horizontal scale ($\varepsilon = 1000$ µm) with a low-pass filter and fitted with the linear model function are assessed here – the surface anisotropy (S_{tr}) and the bearing index (S_{bi}). The former represents the uniformity of the texture aspect and the latter characterizes the quality of the bearing property. In Figure 9(E), the value of S_{tr} shows significant variability in response to the change of the working pressure, which varies between 0.82 and 0.90. As the value of S_{tr} approaches 1, the properties of surfaces are thus isotropic. This finding is coherent in somehow with the observation that sandblasted surfaces do have the same characteristics in all directions (c.f. Fig. 6(A–B)). As for S_{bi}, it is observed to evolve with the pressure in a disordered manner (as seen in Fig. 9(F)), hence it is insensitive to the variation of the pressure. Under

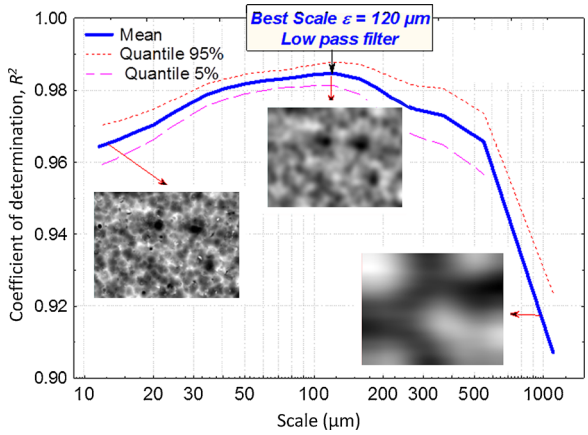

Fig 7. Variation of R^2 as a function of the scale for S_{dq} using a low-pass filter with power law model.

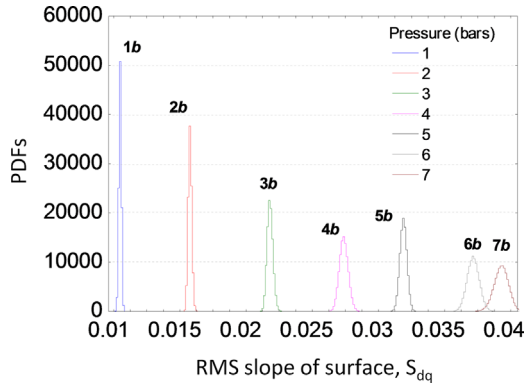

Fig 8. PDFs of S_{dq} modeled with power law function for a cut-off length of 120 using a low-pass filter, under examined working pressures.

the hypothesis of a linear model and with the use of a low-pass filter at full horizontal scale, the parameters S_{tr} and S_{bi} are not suitable for discriminating the pressure effect, where R^2 equals to 0.21 and 0.02 for S_{tr} and S_{bi}, respectively.

Figure 10 represents the (non-normalized) PDF of R^2 for the modeling of S_{dq} and the pressure based on four regression models. The PDFs are exhibited to be fairly in shape and well-fitted by Gaussian bell-curves, i.e., the estimated PDFs of R^2 are quite broad, suggesting that the estimate of R^2 possesses a significant variability. This shows the necessity of using the full PDF of R^2 to discriminate the optimality of the parameter set. A single value of R^2 can give a false decision on the pertinence of the investigated model when it is chosen by chance in the overlapping part of the adjacent PDFs. The power law function is found to have absolute superiority compared to the others.

Discussion

Relevance of the selected roughness parameter

The parameter S_{dq} is exhibited in Figure 5 to be a monotonically increasing function of the pressure. The modeling of arithmetic mean height of surfaces (S_a) and the shortest autocorrelation length (S_{al}) with power law function at 120 µm using a low-pass filter are also found

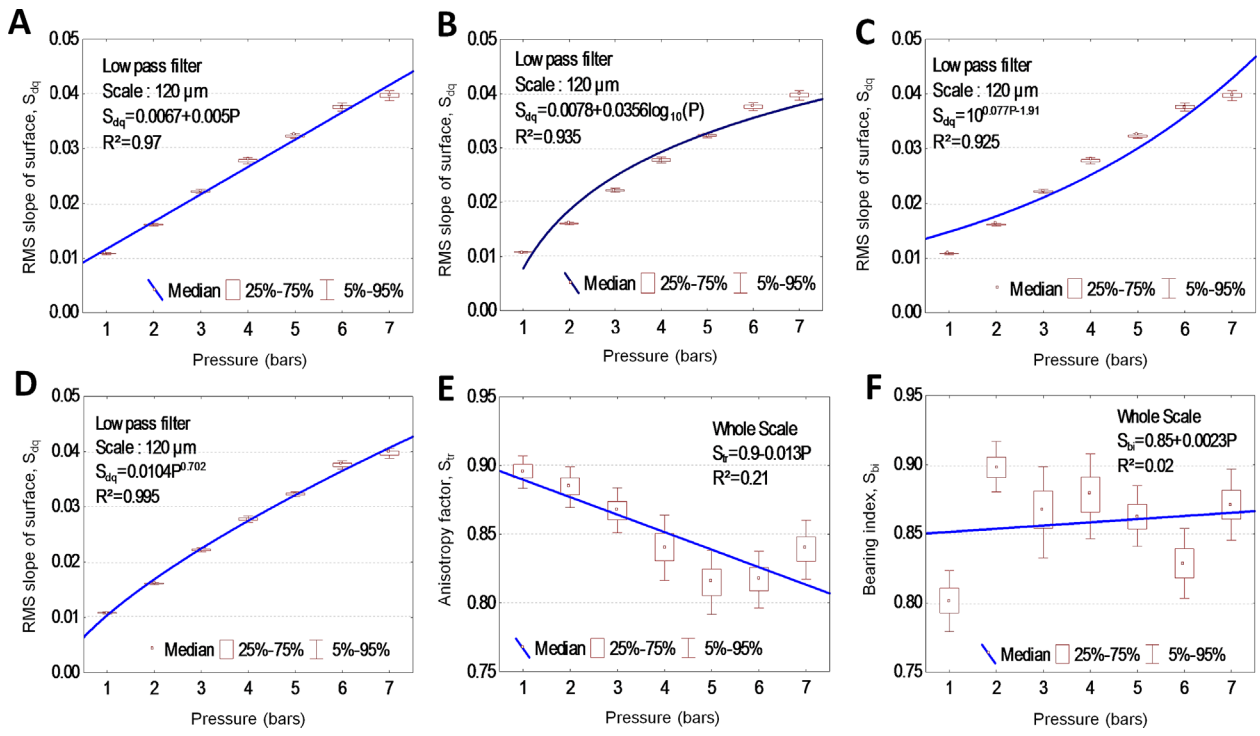

Fig 9. Modeling of S_{dq} with linear (A), logarithmic (B), exponential (C) and power law (D) functions, using a low-pass filter at 120 µm; modeling of S_{tr} (E) and S_{bi} (F) with linear function using a low-pass filter at full horizontal scale.

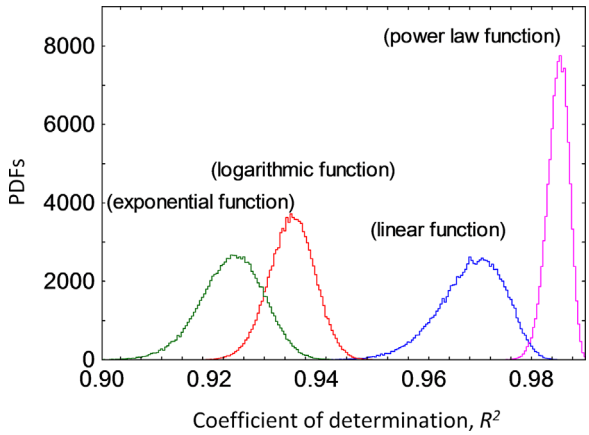

Fig 10. PDFs of R^2 for S_{dq} calculated using a low-pass filter and a cut-off length equal to 120 μm.

to possess similar behavior, as illustrated in Figure 11. It is worth noting that S_a is a widely used roughness parameter due to the simplicity of calculation, the statistical robustness and the ease of interpretation while S_{al}, which is one of the parameters that gives rise to the notion of distance between lumps and bumps, is well adapted to represent the notion of gaps between peaks and valleys in the case of an isotropic surface.

The PDFs of S_{dq} is shown in Figure 8. The PDFs of S_a and S_{al} for the seven examined working pressures are illustrated respectively in Figure 12(A–B); these distributions are well fitted by Gaussian curves. Figure 12(A–B) show that S_a and S_{al} are inappropriate to discriminate pressure effects due to three reasons: I) the values of S_a and S_{al} are particularly large compared to the ones of S_{dq}, II) the dispersion effect is especially pronounced for S_a but notably S_{al} and III) the distributions of S_a and S_{al} overlap each other severely specifically at higher pressures. As for the parameter S_{dq}, the probability distribution of each examined pressure is distinct, indicating that S_{dq} is able to discriminate the pressure effect. In fact, impact craters are formed when SiC particles hit the substrate's surface. The repetitive hitting may cause the formation of a plastically deformed layer and the creation of new craters on the previously formed craters, resulting then in the making of a succession of small peaks and valleys with sharp edges, where their slopes can be characterized by S_{dq}. Indeed, S_{dq} is a 3D hybrid parameter that is described by both the texture amplitude and spacing.

Relevance of the selected scale

The scale of 120 μm, which is demonstrated to be relevant for the parameter S_{dq} in Figure 7, underlines the robustness and accuracy of the methodology proposed in the present study. The scale of 120 μm is situated in the range of the pertinent spectrum with $R^2 \geq 0.90$, covering a band from 15 μm to 1000 μm; the difference between the maximum and the minimum values of R^2 that is equal to 0.085 highlights the accuracy of the proposed methodology with respect to the scale. In this broad-band scale, S_{dq} is dominantly pertinent with $R^2 \geq 0.90$, verifying the robustness of the proposed methodology with respect to the roughness parameter.

Relevance of the selected filter type

The repetitive hitting of abrasive particles on the substrate's surface forms a succession of peaks and valleys with sharp edges; the consideration of an appropriate scale for the measurement of the slopes of these peaks and valleys has been a major problem. Multiple methods are proposed in the literature, for instance, the slope calculation method defined in the standard ISO 25178-2 (2012) and the Lagrangian interpolation polynomial method with seven points in orthogonal directions (Whitehouse and Phillips '82). Although the former method is frequently used, it could not be implemented in the present study as it involves an integral within the definition area of a scale-limited surface. According to the latter method, the computation of the parameter S_{dq} is as follows:

$$S_{dq} = \sqrt{\frac{1}{(M-6)(N-6)} \sum_{j=4}^{N-3} \sum_{i=4}^{M-3} \rho_{ij}^2} \qquad (1)$$

with

$$\rho_{ij} = \left(\left\{ \frac{1}{60\Delta x} \left[-\eta\left(x_{i-3}, y_j\right) + 9\eta\left(x_{i-2}, y_j\right) - 45\eta\left(x_{i-1}, y_j\right) + 45\eta\left(x_{i+1}, y_j\right) - 9\eta\left(x_{i+2}, y_j\right) + \eta\left(x_{i+3}, y_j\right) \right] \right\}^2 + \left\{ \frac{1}{60\Delta y} \left[-\eta\left(x_i, y_{j-3}\right) + 9\eta\left(x_i, y_{j-2}\right) - 45\eta\left(x_i, y_{j-1}\right) + 45\eta\left(x_i, y_{j+1}\right) - 9\eta\left(x_i, y_{j+2}\right) + \eta\left(x_i, y_{j+3}\right) \right] \right\}^2 \right)^{1/2}$$

where $\eta(x_{i+k},y_{i+k})$ is the height coordinate located in (x_{i+k},y_{i+k}), M is the number of points in the profile, N is the number of profiles, and Δx and Δy are the sampling intervals.

Δx *or* Δy, which is the size of the pixel deducted directly from the camera resolution and the field of view, is indirectly pre-defined by the user. S_{dq} is computed by averaging height coordinates at the seven nearest points with a maximum distance of $7\Delta x$ as an evaluation scale, hence only those peaks and valleys with the width in the order of Δx are concerned. At this scale, the high frequency noises generated by e.g. camera measurement noises are quite important, leading to a rather low signal-to-noise ratio. The estimated S_{dq} at this scale is less

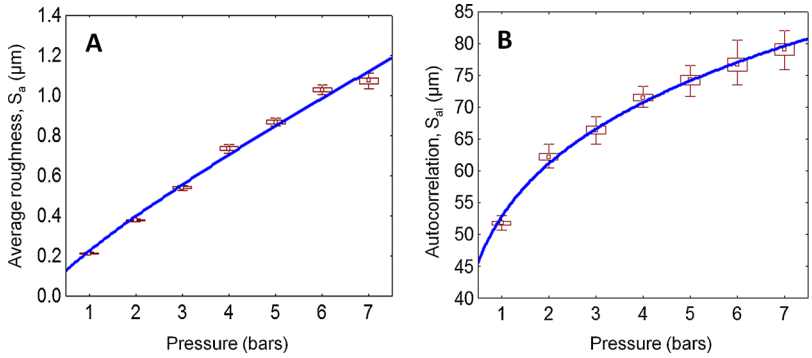

Fig 11. Modeling of S_a and S_{al} with power law function, for a cut-off length of 120 µm using a low-pass filter.

robust as a result. It is therefore important to quantify the variability of the slopes over a wide range of scales using both high-pass and low-pass filters, as represented in Figure 13(A-B), respectively.

In Figure 13(A), the average slope seems to remain constant until they get close to sampling interval. Note that the high pass filter only allows passing the topographic details at finest scales (i.e. the highest spatial frequencies), and therefore, the slope is calculated at these scales in the measurement. Moreover, the calculated results of the slope are likely to contain significant uncertainty, indicating a low accuracy in the estimation of S_{dq} in the presence of strong measurement noise. In Figure 13(B), the average slope is exhibited to be a monotonically increasing function of the scale. This scaling law is shown to be pressure-dependent, i.e. for a given evaluation scale, larger the craters and deeper the indent become when higher the pressure is. Yet, slope differences between the smallest and largest craters tend to become insignificant when the pressure increases. Indeed, the quasi-homogeneous distribution of crater size is obtained at higher pressure condition due to the formation of a hard- and plastically-deformed layer as a consequence of the repetitive hitting of abrasive particles, on which abrasive particles can hardly crush. It is important to note that these results would be the same for any surface that contains some fine scale irregularities.

Relevance of the selected regression model

In what follows, the efficiency of the power law model in describing the correlation between the parameter S_{dq} and the pressure is justified with experimental and theoretical arguments based on the principles of contact mechanics. SiC particles are considered to be elastic spheres of radius D, indenting the elastic subtract to depth h, and thus creating a contact area ($\approx$ craters) with a radius a, it holds that

$$a^2 = Dh \tag{2}$$

Assume S_a to vary in the same way as h, then

$$S_a \propto h \tag{3}$$

The nozzle (working) pressure p can be proportional to the force F applied to the surface, it may then hold that

$$F \propto p \tag{4}$$

According to Johnson ('70),

$$F \propto h^{3/2} \tag{5}$$

By combining Eqs. (3)-(5), it is yielded that

$$S_a \propto p^{2/3} \tag{6}$$

Similarly, it is admitted that S_{al} is proportional to the contact semi-width a,

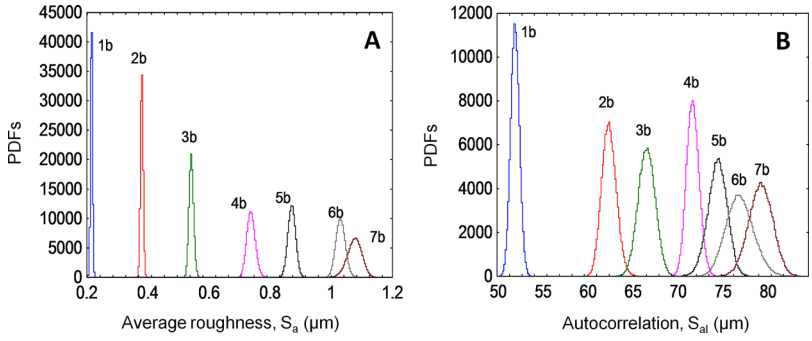

Fig 12. PDFs of S_a (A) and S_{al} (B) modeled with power law function for a cut-off length of 120 using a low-pass filter, under examined working pressures.

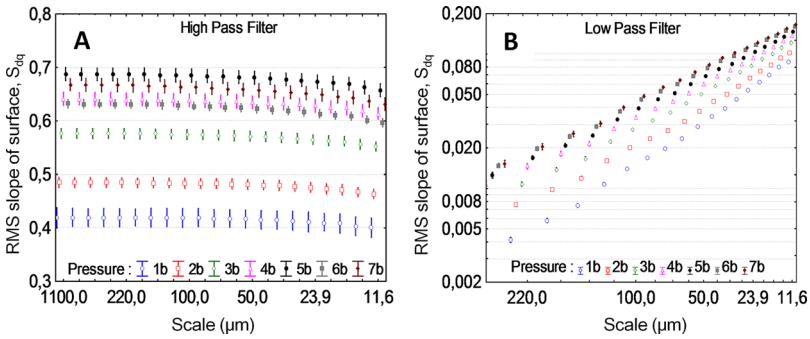

Fig 13. Evolution of S_{dq} versus scale using a high-pass filter (A) and a low-pass filter (B) in the log-log representation.

$$S_{al} \propto a \tag{7}$$

When Eq. (7) is related to Eqs. (2), (4) and (5), the relation between S_{al} and the pressure is

$$S_{al} \propto p^{1/3} \tag{8}$$

It is experimentally demonstrated in Figure 11(A–B) that power law function can be employed to describe the parameters S_a and S_{al} as the function of the pressure:

$$S_a = 0.224p^{0.828} \tag{9}$$

$$S_{al} = 52.81p^{0.211} \tag{10}$$

Assume S_{dq} to be proportional to S_a / S_{al} in an average sense, so

$$S_{dq} \approx 2S_a/S_{al} \tag{11}$$

leading to

$$S_{dq} \propto p^{1/3} \tag{12}$$

When experimental results in Eqs. (9) and (10) are applied to Eq. (11), S_{dq} is written as

$$\begin{aligned} S_{dq} &= 2 \times 0.224p^{0.828}/52.81p^{0.211} \\ &= 0.0085p^{0.611} \approx 0.010p^{0.60} \end{aligned} \tag{13}$$

Experimentally (c.f. Fig. 9(D)),

$$S_{dq} = 0.010p^{0.69} \tag{14}$$

The experimental result in Eq. (14) is exhibited to be remarkably close to the theoretical one in Eq. (13), justifying the approximation made in Eq. (11). Yet, the theoretical function in Eq. (12) seems to be different from the ones in Eq. (13) and Eq. (14), which is mainly due to the following assumption and approximation: (i) the impact of the particles is assumed to be purely elastic, (ii) the superficial friction and particle sliding are neglected. In fact, the relationship defined in Eq. (12) can be refined by formulating the particle impact as a work-energy problem, which however remains challenging to be addressed.It can be concluded that the use of the power law model, suggested by the proposed methodology, to describe the functional relationship between the parameter S_{dq} and the pressure is justified theoretically and experimentally based on the principles of contact mechanics.

Conclusions

The proposed methodology that relies on a multi-scale technique integrated with computer-based bootstrap method has been shown to enable to identify a relevant parameter set for the description of the pressure effect on the sandblasted surface texture. The effect of pressure variation on substrate's texture is found to be best depicted by the roughness parameter called root mean square surface slope (S_{dq}) computed at the scale of 120 µm with a low-pass filter. The relationship between the working pressure and this roughness parameter is exhibited to be best modeled by the power law function with R^2 equal to 0.995; theoretical and experimental analyses based on the principles of contact mechanics are provided for justification.

Acknowledgements

The authors are grateful to the reviewers for their constructive comments, which are valuable for improving the quality of the manuscript.

References

Anselme K, Bigerelle M. 2005. Topography effects of pure titanium substrates on human osteoblast long-term adhesion. Acta Biomater 1:211–222.

Berglund J, Brown CA, Rosen B-G, Bay N. 2010a. Milled die steel surface roughness correlation with steel sheet friction. Annals of CIRP 59/1:577–580.

Berglund J, Agunwamba C, Powers B, Brown CA, Rosen B-G. 2010b. On discovering relevant scales in surface roughness measurement—an evaluation of a band-pass method. Scanning 32:244–249.

Bigerelle M, Najjar D, Mathia T, et al. 2013. An expert system to characterize surfaces morphological properties according to their tribological functionalities: The relevance of a pair of roughness parameters. Tribol Int 59:190–202.

Bouzid S, Bouaouadja N. 2000. Effect of impact angle on glass surfaces eroded by sandblasting. J Eur Ceram Soc 20:481–488.

Brown CA, Siegmann S. 2001. Fundamental scales of adhesion and area-scale fractal analysis. Int J Mach Tools Manuf 41:1927–1933.

Cameron AC, Windmeijer FAG. 1997. An R-squared measure of goodness of fit for some common nonlinear regression models. J Econometrics 77:329–342.

Efron B. 1979. Bootstrap methods: Another look at the Jackknife. Ann Statist 7:1–26.

EUR 15178N. 1993. The development of methods for the characterisation of roughness in three-dimensions″, Commission of the European Communities, EUR 15178 EN.

ISO 25178–2. 2012. Geometrical product specifications (GPS)—Surface texture: Areal—Part 2: Terms, definitions and surface texture parameters.

Johnson KL. 1970. The correlation of indentation experiments. J Mech Phys Solids 18:115–126.

Kim SJ, Kim TH, Kong JH, et al. 2012. Dual-scale artificial lotus leaf fabricated by fully nonlithographic simple approach based on sandblasting and anodic aluminum oxidation techniques. Appl Surf Sci 263:648–654.

Mandelbrot BB. 1977. The fractal geometry of nature. W.H. New York: Freeman and Company.

Mezghani S, El Mansori M, Zahouani H. 2009. New criterion of grain size choice for optimal surface texture and tolerance in belt finishing production. Wear 266:578–580.

Nowicki B. 1985. Multiparameter Representation of Surface Roughness. Wear 102:161–176.

Nwaogu UC, Tiedje NS, Hansen HN. 2013. A non-contact 3D method to characterize the surface roughness of castings. J Mater Process Technol 213:59–68.

Rodrigues Junior SA, Ferracane JF, Della Bona A. 2009. Influence of surface treatments on the bond strength of repaired resin composite restorative materials. Dental Mater 25:442–451.

Shiou F, Asmare A. 2015. Parameters optimization on surface roughness improvement of Zerodur optical glass using an innovative rotary abrasive fluid multi-jet polishing process. Precis Eng 42:93–100.

Vulliez M, Gleason MA, Souto-Lebel A, et al. 2014. Multi-Scale Curvature Analysis and Correlations with the Fatigue Limit on Steel Surfaces after Milling. Proceedings of the CIRP 13:308–313.

Wang H-Y, Zhu R-F, Lu Y-P, et al. 2014. Effect of sandblasting intensity on microstructures and properties of pure titanium micro-arc oxidation coatings in an optimized composite technique. Appl Surf Sci 292:204–212.

Whitehouse DJ. 1994. Handbook of Surface Metrology. Bristol/Philadelphia: Institute of Physics Publishing.

Whitehouse DJ, Phillips MJ. 1982. Two-Dimensional discrete properties of random surfaces. Phil Trans R Soc Lond A 305:441–468.

Xu Z, Liu J, Zhu D, et al. 2015. Electrochemical machining of burn-resistant Ti40 alloy. Chin J Aeronaut. http://dx.doi.org/10.1016/j.cja.2015.05.007

Zhou J, Ai N, Wang L, et al. 2011. Roughening the white OLED substrate's surface through sandblasting to improve the external quantum efficiency. Org Electron 12:648–653.